

Chaotic Dynamics of a Nonlinear Ring Cavity Driven by an External Multi-frequency Signal

A.A. Balyakin, N.M. Ryskin

*Saratov State University, Department of Nonlinear Physics
83, Astrakhanskaya str., Saratov, Russia, 410012
e-mail: BalyakinAA@info.sgu.ru*

Keywords: Chaos; Nonlinear ring cavity; Optical bistability; Ikeda map; Multi-frequency driving

PACS: 42.65.Sf; 47.52+j; 05.45.-a; 0545.Jn

1 Introduction

A nonlinear ring cavity driven by an external signal is among the most popular models of nonlinear dynamics [1, 2]. A special attention to this system is paid in non-linear optics where it was considered for the first time by Ikeda and co-authors [1–5]. Many interesting non-linear phenomena such as bistability, transitions to chaos, and pattern formation have been studied both theoretically and experimentally (see for details [6–8]). Those researches are of great interest because of prospects to apply bistable cavities as logical elements in optical computers and in cryptography [6, 7, 9, 10]. We note that similar systems can be also produced not only in optics, but also in microwave diapason.

Schematic drawing of studied device is presented in Fig. 1. A nonlinear dielectric with Kerr-type nonlinearity is placed inside a ring optical cavity. The cavity is excited by an input signal $E_0(t)$ from an external laser source. However, we do not restrict ourselves to the nonlinear optical system. Our analysis is valid for any type of waves propagating in a nonlinear medium with cubic phase nonlinearity when output signal is partly recirculated to the input through a feedback loop.

For the case of harmonic input signal the behavior of the system has been studied thoroughly [1–8, 11]. Under several assumptions (plane wave approximation, neglecting dispersion and losses in the nonlinear media, etc.) a simple return map can be derived to describe the dynamics of complex amplitude of the signal

$$A_{n+1} = A_0 + \rho A_n \exp(i|A_n|^2 + i\varphi). \quad (1)$$

Here A_n is the signal amplitude on n -th spreading through the cavity, A_0 is a constant amplitude of the input signal, ρ is an amount of feedback ($0 < \rho < 1$), and φ is a total phase shift of the signal for a single spreading through the feedback loop. The map (1) is known as *Ikeda map*. For sufficiently high input power the steady-state single frequency oscillations become unstable and periodic pulsations arise with the period equal to doubled delay time [1–8]. This phenomenon is called Ikeda instability. The subsequent increase of the input signal leads to transition to chaos by Feigenbaum scenario and then to formation of Ikeda attractor [3, 4] that corresponds to the fully-developed, strongly irregular chaotic motion.

In this paper, we investigate nonlinear dynamics of this system when the input signal is multi-frequency, containing several discrete spectral components $\omega_1, \omega_2, \dots, \omega_n$:

$$E_0 = \sum_{j=1}^n A_{0j} \exp(i\omega_j t) + \text{c.c.}, \quad (2)$$

where A_{0j} are complex constant amplitudes, c.c. denotes complex conjugate. For the sake of simplicity we suppose the frequencies ω_j to be non-resonant, i.e. their ratios are irrational numbers, and restrict ourselves to double-frequency driving, $n = 2$. Note that similar problem (for $n = 2$ or 3) have been already considered in [12]. However, in cited work the main concern was with the steady-state characteristics of the device in the case of symmetrical pumping (i.e. equal input intensities for both frequencies). In contrast to [12] we will focus on case when the pumping is strongly asymmetric, treating the second signal as a small control action. Our aim is to demonstrate that varying the intensity of the second signal opens a possibility to effective control of the dynamics of the primary signal. We also will concentrate on the transitions to chaos and on peculiarities of the chaotic oscillations. Some preliminary results presented in [13, 14] show that the chaotic dynamics can be much more diverse than for the single-frequency driving.

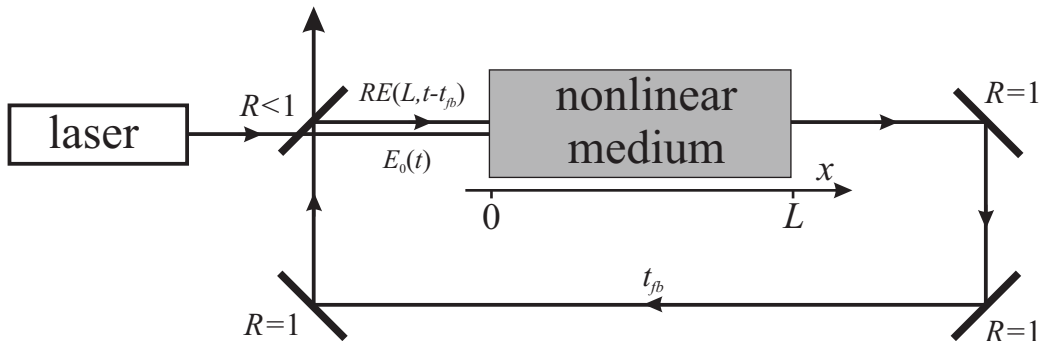


Figure 1: Schematic drawing of a nonlinear ring cavity under external driving

The paper is organized as follows. In Sec. 2, the derivation of the coupled Ikeda maps is described in details. Although the equations are obtained for a general case of an arbitrary number of input frequencies, further the double-frequency driving is considered. The stability analysis of obtained equations is performed in Sec. 3. Results of numerical simulations of non-stationary oscillations are presented in Sec. 4. Various types of transitions to chaos are discovered while the input signal power is increased. Sec. 5 contains some concluding remarks.

2 Derivation of coupled Ikeda maps

To describe the propagation of a multi-frequency wave packet in a nonlinear medium we use the Hamiltonian formalism that is one of the most powerful tools in the theory on non-linear wave interaction (for review see [15]). We assume that only one type of waves should be considered, with dispersion relation $\omega = \omega(k)$ that does not admit three-wave resonant interactions. Thus, first-order nontrivial nonlinear processes are caused by four-wave interactions, and Hamiltonian of the system can be written as follows [15]:

$$H = H_0 + H_{int} + \dots, \quad (3)$$

$$H_0 = \int \omega(k) a_k a_k^* dk, \quad (4)$$

$$H_{int} = \frac{1}{2} \int T_{k_1 k_2 k_3 k_4} a_{k_1}^* a_{k_2}^* a_{k_3} a_{k_4} \delta(k_1 + k_2 - k_3 - k_4) dk_1 dk_2 dk_3 dk_4. \quad (5)$$

Here H_0 is a linear part of Hamiltonian, H_{int} describes nonlinear interactions. In (3)-(5) a_k is a Fourier amplitude of the wave with wavenumber k , δ is the Dirac delta-function, $T_{k_1 k_2 k_3 k_4}$ is a four-wave interaction matrix element (see [15] for more details).

For the input signal (2) we suppose the field to be presented as a multi-frequency wave packet consisting of several discrete spectral components

$$E = \sum_{j=1}^n A_j(x, t) \exp(i\omega_j t - ik_j x) + \text{c.c.}, \quad (6)$$

with frequencies ω_j and wavenumbers k_j being connected with each other by dispersion relation $\omega_j = \omega(k_j)$ and A_j being the slow varying (in comparison with complex exponents) envelope amplitudes. If all the frequencies are non-resonant, i.e. none of the conditions

$$\sum_j N_j \omega_j = 0$$

holds true for integer N_j , one can show that propagation of the wavepacket (6) is governed by the system of coupled non-linear Schrödinger equations [16]

$$i \left(\frac{\partial A_j}{\partial t} + V_g^j \frac{\partial A_j}{\partial x} \right) + \frac{\omega_j''}{2} \frac{\partial^2 A_j}{\partial x^2} + \left(\beta_{jj} |A_j|^2 + \sum_{j \neq i} \beta_{ji} |A_i|^2 \right) A_j = 0. \quad (7)$$

Here $V_g^j = \left. \frac{d\omega}{dk} \right|_{k=k_j}$ are the group velocities, $\omega_j'' = \left. \frac{d^2\omega}{dk^2} \right|_{k=k_j}$ are the parameters of group velocity dispersion, and coefficients β responsible for non-linear interaction between waves with different components of the wave packet are defined as follows:

$$\beta_{jj} = -2T_{k_j k_j k_j k_j}, \quad \beta_{ji} = - \left(T_{k_j k_i k_j k_i} + T_{k_j k_i k_i k_j} + T_{k_i k_j k_j k_i} + T_{k_i k_j k_i k_j} \right). \quad (8)$$

Further we shall neglect the effects of group velocities dispersion ($\omega_j'' = 0$, $V_g^j \equiv V_g$). Hence, the equations (7) transforms into

$$i \left(\frac{\partial A_j}{\partial t} + V_g \frac{\partial A_j}{\partial x} \right) + \left(\beta_{jj} |A_j|^2 + \sum_{j \neq i} \beta_{ji} |A_i|^2 \right) A_j = 0. \quad (9)$$

One can easily find the solution of (9) in the form

$$A_j(x, t) = A_j \left(0, t - \frac{x}{V_g} \right) \exp \left\{ \frac{ix}{V_g} \left[\beta_{jj} \left| A_j \left(0, t - \frac{x}{V_g} \right) \right|^2 + \sum_{j \neq i} \beta_{ji} \left| A_i \left(0, t - \frac{x}{V_g} \right) \right|^2 \right] \right\}. \quad (10)$$

Since the total field at the input of the non-linear medium (at $x = 0$) is composed by the external driving signal and the signal traveled through the resonator (see Fig. 1) the boundary condition is the following

$$E(0, t) = E_0 + RE(L, t - t_{fb}). \quad (11)$$

Here t_{fb} is the time of signal propagation in the feedback loop, L is the length of the non-linear medium, and R is (generally complex) feedback parameter which is assumed to be the same for all frequencies. For the case of an optical ring cavity shown in Fig. 1 R is the reflectivity of the output mirror (other three mirrors are assumed to have $R = 1$).

Substituting (2), (6), and (10) into (11) we obtain a system of delayed equations (cf. [5–8])

$$A_j(t + \tau) = A_{0j} + \rho A_j(t) \exp \left[i \left(\frac{\beta_{jj}L}{V_g} |A_j(t)|^2 + \sum_{i \neq j} \frac{\beta_{ji}L}{V_g} |A_i(t)|^2 + \varphi_j \right) \right], \quad (12)$$

where $\tau = t_{fb} + l/V_g$ is the time delay, $\rho = |R|$, $\varphi_j = \text{Arg}(R) - \omega_j \tau$ are total phase shifts for a single spreading through the feedback loop, that in general are different for different spectral components. Note that the phase space of the system of time delayed equations (or functional maps) (12) is infinite-dimensional. Our next step is to turn to a more simple system of coupled return maps. Examining the output signal dynamics in discrete moments of time $t_n = n\tau$ yields a system of coupled Ikeda maps

$$A_j^{n+1} = A_{0j} + \rho A_j^n \exp \left[i \left(\frac{\beta_{jj}L}{V_g} |A_j^n|^2 + \sum_{i \neq j} \frac{\beta_{ji}L}{V_g} |A_i^n|^2 + \varphi_j \right) \right], \quad (13)$$

where $A_j^n = A_j(t_n)$.

We restrict ourselves now to the investigation of two-frequency external signal. In that case we obtain from (13)

$$\begin{aligned} A_1^{n+1} &= A_{01} + \rho A_1^n \exp \left[i \left(|A_1^n|^2 \frac{\beta_{11}L}{V_g} + |A_2^n|^2 \frac{\beta_{12}L}{V_g} + \varphi_1 \right) \right], \\ A_2^{n+1} &= A_{02} + \rho A_2^n \exp \left[i \left(|A_2^n|^2 \frac{\beta_{22}L}{V_g} + |A_1^n|^2 \frac{\beta_{21}L}{V_g} + \varphi_2 \right) \right]. \end{aligned} \quad (14)$$

Let us suppose all four-wave interaction matrix elements to be equal: $T_{k_1 k_2 k_3 k_4} = T$. Thus, equations (8) give $\beta_{jj} \equiv \beta = -2T$, $\beta_{ji} = -4T = 2\beta$. Finally, to minimize the number of significant parameters we make in (14) the following change of variables: $A_j \rightarrow A_j / \sqrt{\beta L / V_g}$, $A_{0j} \rightarrow A_{0j} / \sqrt{\beta L / V_g}$. As a result we obtain

$$\begin{aligned} A_1^{n+1} &= A_{01} + \rho A_1^n \exp \left[i \left(|A_1^n|^2 + 2 |A_2^n|^2 + \varphi_1 \right) \right], \\ A_2^{n+1} &= A_{02} + \rho A_2^n \exp \left[i \left(|A_2^n|^2 + 2 |A_1^n|^2 + \varphi_2 \right) \right]. \end{aligned} \quad (15)$$

Since the variables A_j^n are complex, the phase space of this system is four-dimensional. Note that in the absence of the second signal, $A_{02} = 0$, (15) can be reduced to the single Ikeda map (1).

We recall that coupled return maps (15) derived in 2 performs simple model (we used plane wave approximation, neglected dispersion and losses in the nonlinear media, etc.). Exact solution of coupled Schrödinger equations (7) is also possible and will be presented hereafter. We will not discuss here the difference between two approaches either. Some remarks concerning differential equations with time-delayed feedback can be found in, e.g. [17–20]

3 Stationary regimes and stability analysis

As *stationary regimes* we name henceforth the oscillation when signal amplitudes are time-independent. That corresponds to stable points of coupled Ikeda maps $A_j^n = A_j^0 = \text{const}$. For stationary intensities $I_j = |A_j^0|^2$ we have

$$I_1 = \frac{I_{01}}{1 + \rho^2 - 2\rho \cos \Phi_1}, \quad (16)$$

$$I_2 = \frac{I_{02}}{1 + \rho^2 - 2\rho \cos \Phi_2}, \quad (17)$$

here $I_{0j} = |A_{0j}|^2$ — intensities of outgoing signals; $\Phi_i = I_i + 2I_j + \varphi_i$, $i, j = 1, 2$. Equations (16), (17) are transcendental and can be solved only numerically. Fig. 2 represents the dependence $I_1(I_{01})$ — gain characteristics.

Dashed lines correspond to $I_{01}/(1 \pm \rho)^2$, that is the limits of $I_{1,2}$:

$$\frac{I_{0j}}{(1 + \rho)^2} < I_j < \frac{I_{0j}}{(1 - \rho)^2}. \quad (18)$$

Fig.2a corresponds to the case when the second signal is absent, $I_{02} = 0$, and is analogous to well-known gain characteristics of nonlinear ring cavity presented in, e.g., [7]. That diagram evidently illustrates the phenomena of multi-stability and hysteresis, peculiar to discussed system. The branches with negative incidence comply to unstable states. Arrows denote shifts from one stable branch of gain characteristics to another.

The increase of the second signal intensity leads to the complication of $I_1(I_{01})$, number of branches also increases (Fig.2c). We note, that there exist stable part of gain characteristics, that can not be arrived by smooth varying of I_{01} (they are marked with dots). To obtain these regimes one should either provide very precise starting conditions or move in parameter space in very particular direction. Thus nonstationary dynamics of the system is expected to be much more diverse comparatively to single Ikeda map. We emphasize that in all cases performed in Fig.2 the intensity of the second component remains rather small sofar it can be treated as weak control action ($I_{02} < 0.36$, compare with I_{01}).

Now let us undertake the stability analysis of stationary solutions. Linearizing the maps in the vicinity of a stable point after simple but bulky transformations we derived characteristic equation:

$$[\mu^2 - 2\mu\rho(\cos \Phi_1 - I_1 \sin \Phi_1) + \rho^2][\mu^2 - 2\mu\rho(\cos \Phi_2 - I_2 \sin \Phi_2) + \rho^2] = 16\mu^2\rho^2 I_1 I_2 \sin \Phi_1 \sin \Phi_2. \quad (19)$$

here μ — multiplier. We note that terms in brackets in the left part of (19) coincide with characteristic equations for single Ikeda map (1). Consequently we interpret the right-hand term as a coupling parameter.

The loss of stability can happen in a various ways (see for details, e.g., [21]): as a result of doubling period bifurcation ($\mu = -1$), tangent bifurcation ($\mu = 1$), as well as Neimark bifurcation (the last corresponds to two complex conjugate multipliers $\mu_{\pm} = \exp(\pm i\theta)$). We plot the lines of different bifurcations on a parameter plane (A_{01}, φ_1) , analyzing equation (19) numerically. We note that negatively inclined branches are unstable owing to tangent

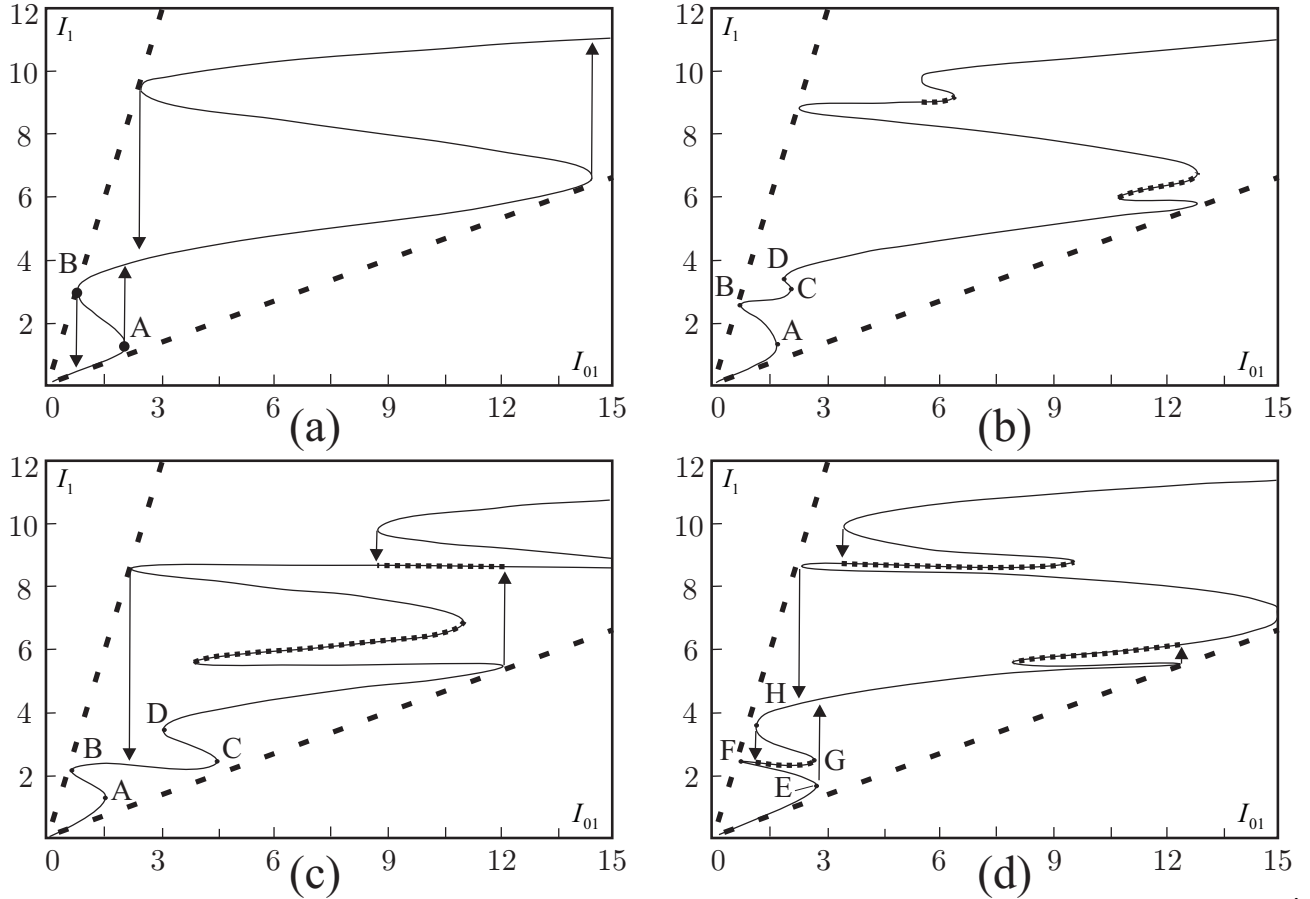


Figure 2: Gain characteristics for coupled Ikeda maps. $\varphi_1=\pi$, $A_{02}=0$ (a), $A_{02}=0.4$ (b), $A_{02}=0.6$ (c), $A_{02}=0.6$, $\varphi_1=3\pi/4$ (d)

bifurcation. Thus lines $\mu = 1$ in a parameter plane limit the regions of multi-stability and hysteresis.

Results of numerical solution (19) are performed in Fig.3. Solid lines denote first doubling bifurcations, interrupted lines correspond to tangent bifurcations, and dotted lines – to Neimark bifurcation. Vertical lines correspond to directions along which gain characteristics, presented in Fig.2, were plotted. Letters A,B,...H mark rough transitions between different branches. As seen from Fig.3 they coincide with hysteresis region, i.e. tangent bifurcation. Varying of the second signal phase φ_2 does not influence dramatically the dynamics of the system, therefore we restrict our numerical analysis to the case when $\varphi_2 = 0$. All results are periodic in φ_1 with period equal to 2π .

Fig. 3a corresponds to Ikeda map. One observes the borders of hysteresis region and doubling bifurcation line. When amplitude of the second signal is rather small, there are no noticeable changes in a parameter plane. The last can be observed only when A_{02} increases to 0.4. There appear the regions of quasi-periodic motion inside the region, limited by Neimark bifurcation lines (fig 3c). With the increase of I_{02} they grow in size, and there exist two those regions, dwelling in different sheets of a parameter plane (fig 3d).

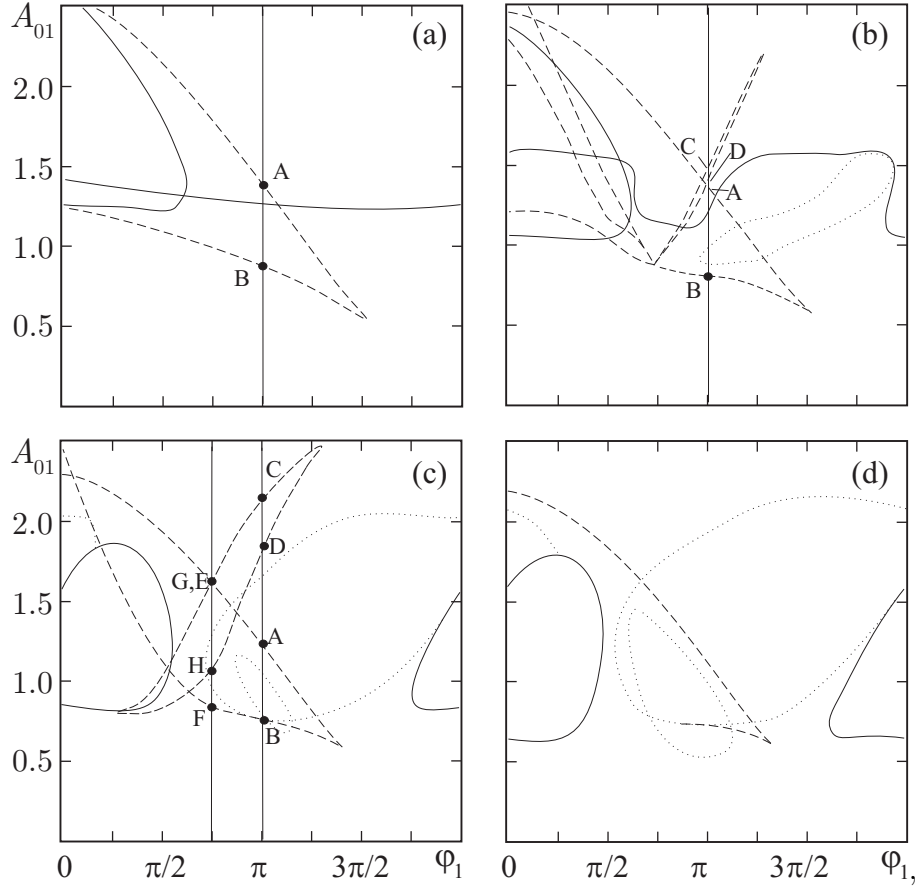


Figure 3: Lines of different bifurcations on a parameter plane: first doubling bifurcation (solid lines), tangent bifurcation (dash lines), Neimark bifurcation(dotted lines).Parameters: $\rho = 0.5$, $\varphi_2 = 0$, and $A_{02} = 0.0$ (a), 0.4 (b), 0.6 (c), 0.8 (d). Thin lines correspond to direction along which gain characteristics on Fig.2 were built

4 Results of Numerical Modelling and Discussion

To investigate nonlinear dynamics of the coupled Ikeda maps (15) we performed numerical simulation in a wide range of parameters. Our primary goal is to demonstrate that adding the second signal component could cause qualitative changes in the dynamics of the system in comparison to the single-frequency driving. In Fig. 4 the typical results are presented as bifurcation charts (phase diagrams) in the plane (A_{01}, φ_1) for different values of A_{02} . The choice of the parameters A_{01} and φ_1 (that have meaning of external driving magnitude and frequency, respectively) is quite natural for non-autonomous nonlinear oscillator. The pictures are periodic in φ_1 with the period 2π . The phase of the second signal φ_2 does not strongly affect the dynamics of the system and leads mainly to shift of the bifurcation lines along the φ_1 axes. Henceforth all the presented results correspond to the case $\varphi_2 = 0$.

In Fig. 4 the regions of periodic oscillations with different periods, quasi-periodic oscillations, and chaotic ones are shown. In each point on the parameter plane we determine the type of dynamical regime after sufficiently long transient process. For that purpose we use phase portraits, power spectra, and spectra of Lyapunov exponents. In the regions of periodic motion

all the exponents are negative, for quasi-periodic motion there are one zero and three negative exponents, while in chaotic regimes one of the exponents becomes positive [?, 2, 21]. We chose the direction of scanning on the parameter plane to be bottomup and from left to right and use the hereditary of initial conditions. The last means when the transient process is over and the dynamical regime in a point on the parameter plane is determined we increase smoothly the value of the phase shift φ_1 taking the current values of variables as initial conditions for a new point. When φ_1 reaches the limit $\varphi_1 = 2\pi$ we increase slightly the value of A_{01} and return to $\varphi_1 = 0$. Note that owing to the bistability the bifurcation charts are multi-folded, and only the parts corresponding to the lower branch of the cavity transfer function are shown in Fig. 4. To obtain the other parts of the charts one should vary the scanning direction.

The bifurcation chart for $A_{02} = 0$ (Fig. 4(a)) coincide with that for the single Ikeda map (1), when built in appropriate coordinates (see, for example [23], Figs. 3(b),4(b))¹. In Fig. 4(a) one can see the regions of period doublings and transition to chaos via Feigenbaum scenario. We show only the first two doubling bifurcations that are depicted with thin solid lines. The domains of higher order bifurcations are not shown because of their small sizes. In the region of chaotic motion there exist many domains of periodic oscillations, which have a form known as “*crossroad area*” [21, 23]. The large ones (with periods 3 and 4) are shown in Fig. 4(a). The exit from crossroad areas occurs via Feigenbaum scenario.

For small enough amplitude of the second signal A_{02} (Fig. 4(b)) the changes in the bifurcation chart compared with Fig. 4(a) are hardly noticeable. Only slight deformation of the borders of the oscillations of different types is observed.

With increasing of A_{02} the bifurcation lines become more complicated. Furthermore, in contrast to a single Ikeda map, quasi-periodic motion can take place (Fig. 4(c,d)). The quasi-periodic domains contain a large number of synchronization tongues; the largest ones are shown in Fig. 4(c,d,e). Inside the tongues the motion is periodic with rational winding numbers (the values of the winding numbers are indicated in Fig. 4). We emphasize that the winding number changes smoothly while moving in the quasi-periodic domains. For example, in the domain adjoining the region of periodic oscillations with period 1 in Fig. 2(c), the winding number varies from 1 to 1/2, and there exist all synchronization tongues corresponding to the rational winding numbers within the limits of variation. For sufficiently large A_{02} (Fig. 2(d,e)) quasi-periodic route to chaos (Ruelle–Takens scenario) becomes possible.

It should be pointed out that variables $A_{1,2}$ are the envelope amplitudes of spectral components with frequencies $\omega_{1,2}$. Since a stable fixed point of the map (15) describes a steady-state solution when the amplitudes are time-independent, $A_{1,2} = \text{const}$, the real physical field $E(x, t)$ (6) in general case (for the frequencies $\omega_{1,2}$ supposed to be non-resonant, see Sec. 2) exhibits quasi-periodic oscillations with two independent frequencies, in contrast to the single Ikeda map (1) where steady-state solution corresponds to periodic oscillations with frequency of external driving. In non-stationary regimes when the amplitudes $A_{1,2}$ vary in time, both components of the output signal become modulated. We presume the carrier frequencies $\omega_{1,2}$ to be sufficiently far off from each other ($|\omega_1 - \omega_2| \gg 2\pi/\tau$, τ is the time delay), so their modulation spectra do not intersect. So, dealing with an experimental device, it is possible to investigate the dynamics of each component separately using a band-pass filter tuned on one of the carrier frequencies.

When the first period doubling bifurcation occurs (appearance of a 2-period cycle from a

¹In Ref. [23] the bifurcation charts are built in the plane of parameters that correspond to A_0 and $1/\varphi$ in the equation (1). After appropriate redrawing one can demonstrate that the maps become 2π -periodic in φ .

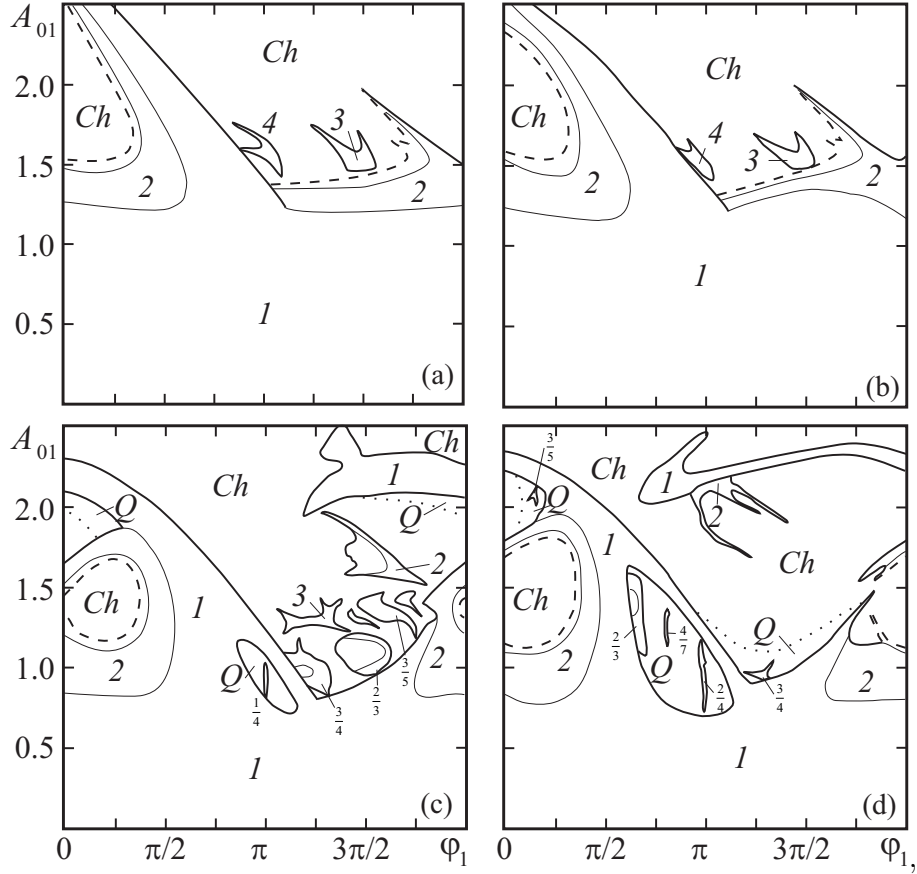


Figure 4: Bifurcation charts on the plane of parameters (A_{01}, φ_1) for $\rho = 0.5$, $\varphi_2 = 0$, and $A_{02} = 0.0$ (a), 0.2 (b), 0.6 (c), 0.8 (d). Transitions to chaos via Feigenbaum scenario are shown by dashed lines; quasi-periodic transitions to chaos are shown by dotted lines; period doubling bifurcations are shown by thin solid lines. Only first two bifurcations are depicted, higher-order ones are not shown for the lack of space. *Ch* — regions of chaotic oscillations *Q* — regions of quasi-periodic oscillations, numbers mark regions of periodic oscillations with corresponding period. For synchronization tongues the values of winding number are indicated.

stable point), the amplitudes exhibits periodic self-pulsations with period 2τ . Therefore, this bifurcation corresponds to the oscillatory Ikeda instability caused by the delayed feedback [1–5]. The spectrum contains side-bands (satellites) with frequencies $\omega_{1,2} \pm n\omega_I$, $n = 1, 2, \dots$, where $\omega_I = \pi/\tau$ — the self-modulation frequency. During transition to chaos the spectrum is enriched by new sub-harmonic components with frequencies $\omega_{1,2} \pm n\omega_I/2^m$.

On the contrary, in the quasi-periodic regime a fixed point loses its stability via the Hopf bifurcation, when a unit circle is crossed by a pair of complex conjugate multipliers and an attractor is invariant curve [1, 2, 21]. The side-band frequencies are $\omega_{1,2} \pm n\omega_Q$ with $\omega_Q \neq \pi/m\tau$. For the dynamics of the total field $E(x, t)$ (6) it corresponds to periodic amplitude self-pulsations with period different from 2τ , and the attractor is a 3D torus with three independent frequencies (two carrier frequencies $\omega_{1,2}$ and that of the self-pulsations, ω_Q). Inside the synchronization tongues ω_Q is commensurable to the Ikeda frequency ω_I , i.e. a winding number $w = \omega_Q/\omega_I$ is rational, $w = p/q$, p and q — integer. The single Ikeda map (1) does not exhibit the Hopf bifurcation and quasi-periodic motion [1–5, 8, 21, 23]. Hence, we obtain a new type of insta-

bility caused by nonlinear interaction of two driving signal components, i.e. by phase cross-modulation. Note that the effects of phase cross-modulation are very important in nonlinear optics, particularly for wave propagation in optical fibers [24].

We point out that the results of direct computer modelling of (1) are of great agreement with the analysis of characteristic equations undertaken in Sec. 3. Some distinctions are connected with the choice of scanning direction.

We observe three different routes to chaos: Feigenbaum period doubling scenario, quasi-periodic (Ruelle–Takens) scenario, and hard transition. Accordingly, three types of chaotic attractors exist (Fig. 5). We use the following notation: C_F for the Feigenbaum attractor originated from period doubling bifurcation sequence, C_Q for the one formed from quasi-periodic motion, and C_I for the well-known Ikeda attractor [5] that exists for high pumping levels and corresponds to fully-developed, strongly irregular chaotic motion. The three described types differ not only in visual appearance, but also in signature of Lyapunov exponents: C_Q -type attractor has one positive, one zero, and two negative exponents, while C_F and C_I types have one positive and three negative exponents. No hyperchaotic regimes with two positive exponents occur. We emphasize that for the single Ikeda map (1) only C_F and C_I types exist and quasi-periodic route to chaos never takes place. We represent in Fig.5 Feigenbaum-type attractor (a), C_F ($\varphi_1 = \pi/6$, $A_{01} = 1.3$); (b) attractor originated from the quasi-periodic route to chaos, C_Q ($\varphi_1 = 3\pi/2$, $A_{01} = 1.5$); (c) Ikeda-type attractor, C_I ($\varphi_1 = \pi$, $A_{01} = 2.5$). Other parameters are the same as for Fig. 4(c).

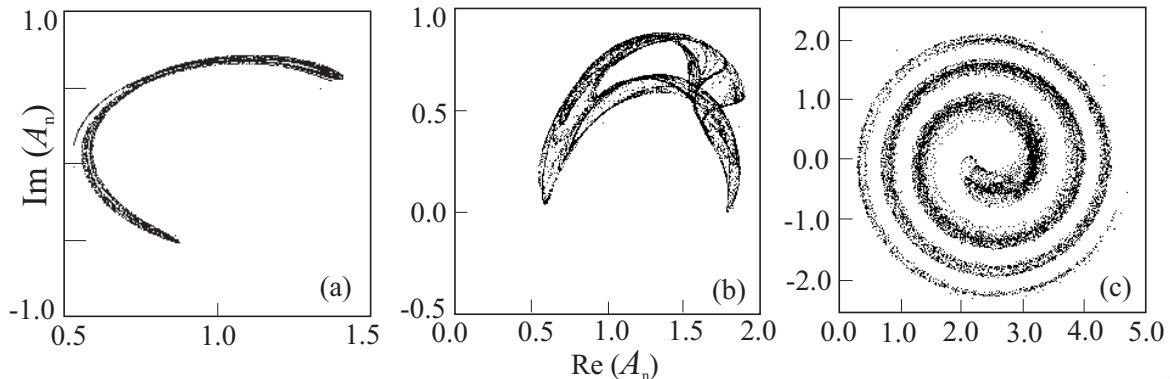


Figure 5: Chaotic attractors of different types

From Fig. 3 one can see that the bifurcation charts are very complicated, and thus, a great variety of bifurcation sequences could be observed while moving in different ways on the parameter plane. For better understanding the behavior of the system we built single-parameter bifurcation diagrams: $Re(A_n^1)$ plots versus A_{01} . Some examples are presented in Fig. 6 for different values of φ_1 . All diagrams are plotted with smooth increase of A_{01} with hereditary of initial conditions for $\varphi_1 = \pi/6$ (a), $\varphi_1 = \pi$ (b), and $\varphi_1 = 3\pi/2$ (c). Other parameters are the same as for Fig. 4(c).

The first diagram (Fig. 6(a)) shows period doubling bifurcations and transition to chaos via Feigenbaum scenario at $A_{01} \approx 1.2$. In the region of chaotic motion several windows of periodicity are clearly seen. At $A_{01} \approx 1.5$ the C_F -type attractor begins to transform in the C_I -type one. When $A_{01} \approx 1.63$ one observes a hard transition between different types of chaotic oscillations known as a crisis of chaotic attractors. In that case chaotic attractor

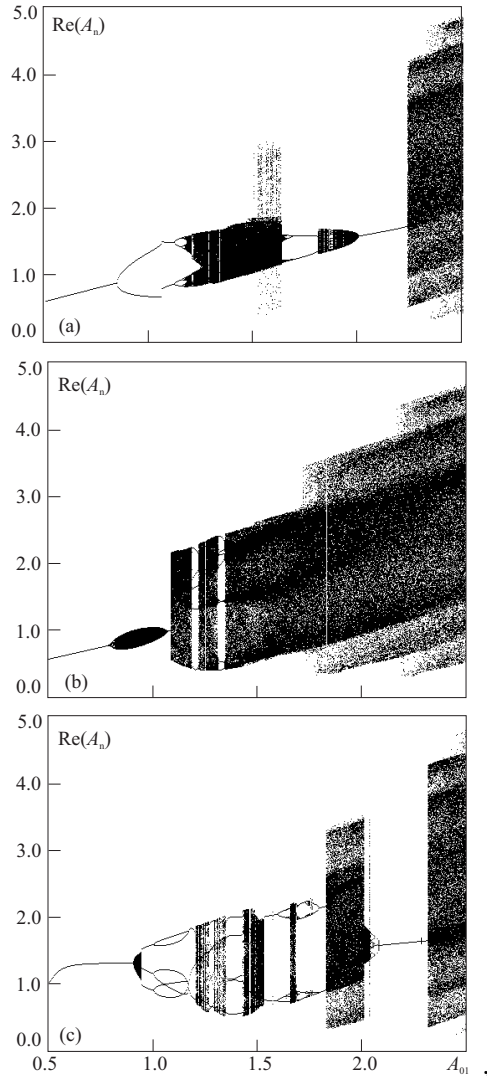


Figure 6: Single-parameter bifurcation diagrams $Re(A_n^1)$ versus A_{01}

abruptly expands or contrarily shrinks, that is explained by its collision with non-stable periodic orbit [21, 22]. Further increase of A_{01} leads to the reverse doubling bifurcation sequence. At $A_{01} \approx 1.8$ a hard transition to quasi-periodic motion takes place. Inside the region of quasi-periodicity one can see several windows of synchronization. With increase of A_{01} the quasi-periodic attractor shrinks, and at $A_{01} \approx 2.0$ the motion again becomes periodic. Finally, the hard transition to Ikeda attractor C_I takes place at $A_{01} \approx 2.25$.

On the second diagram (Fig. 6(b)) one can see a region of quasi-periodic oscillations that appears and disappears softly (i.e. via direct and reverse Hopf bifurcations) at $A_{01} \approx 0.8$ and $A_{01} \approx 1.1$, respectively. Hard transition to chaotic attractor C_I occurs at $A_{01} \approx 1.25$. Subsequent increase of A_{01} causes the expansion of the attractor C_I .

The bifurcation diagram presented on Fig. 4(c) illustrates soft appearance of quasi-periodic oscillations ($A_{01} \approx 0.9$). A number of synchronization windows with different periods can be observed, inside some of them period doublings takes place. At $A_{01} \approx 2.0$ a crisis of chaotic attractors is clearly visible. The bifurcation sequence ends with a hard transition to Ikeda

attractor at $A_{01} \approx 2.3$.

5 Concluding remarks

In this paper, we discussed an extension of the Ikeda system for the case of multi-frequency external signal. The system of coupled Ikeda maps was derived to describe the dynamics of slowly varying amplitudes of spectral components. For the simplest case of double-frequency driving results of numerical simulation were presented, that confirm that the dynamics is much more diverse than for the single-frequency driving. Various transitions to chaos were observed: the Feigenbaum period doubling scenario, quasi-periodic (Ruelle–Takens) scenario, hard transition to chaos, and crisis of chaotic attractors. Applying of the second input signal gives the opportunity to efficient control of the dynamics of the system. Changing amplitude and phase of the second signal component one can either suppress the chaotic oscillations or conversely cause the steady-state oscillations to be unstable. These results are significant for prospects to use nonlinear ring cavities as logical elements in optical computers [7].

However, the validity of the model (15) needs further consideration, since a number of simplifying assumptions has been made. First of all, we neglected transverse effects (diffraction, self-focusing, etc.) that lead to a wide class of transversal instabilities [7, 8]. We also did not take into account group velocity dispersion effects that may cause modulation (Benjamin–Feir) instability and formation of solitons [7, 24]. All these phenomena usually play an important role in nonlinear optics, and their consideration will be a subject of further investigation.

Finally, we note that Ikeda map describes non only a nonlinear ring cavity, but also many other interesting physical systems, e.g. a periodically kicked nonlinear oscillator [23]. Evidently, the system of coupled maps (15) can be derived for a quasi-periodically kicked oscillator.

6 Acknowledgements

This work was supported by USA Civilian Research and Development Foundation (Award No REC-006) and Russian Foundation for Basic Research (grants No. 02-02-16351 and 02-02-06315).

References

- [1] Yu.I. Neimark, P.S. Landa, Stochastic and Chaotic Oscillations, Kluwer, Dordrecht, 1992.
- [2] P.S. Landa, Non-Linear Oscillations and Waves in Dynamical Systems, Kluwer, Dordrecht, 1996.
- [3] K. Ikeda Multiple-valued stationary state and its instability of the transmitted light by a ring cavity system // Opt. Comm. **30** (1979) 257
- [4] K. Ikeda, H. Daido, O. Akimoto .Optical turbulence: chaotic behavior of transmitted light from a ring cavity // Phys. Rev. Lett. **45** (1980) 709.

- [5] K. Ikeda, O. Akimoto Instability leading to periodic and chaotic self-pulsations in a bistable optical cavity // *Phys. Rev. Lett.* **48** (1982) 617.
- [6] H.M. Gibbs, *Optical Bistability: Controlling Light with Light*, Academic, New York, 1985.
- [7] N.N. Rosanov, *Optical Bistability and Hysteresis in Distributed Non-Linear Systems*, Nauka, Moscow, 1997.
- [8] J.V. Moloney, A.C. Newell *Nonlinear optics* // *Physica D* **44**, (1990) 1.
- [9] X.Wang, M.Zhan, X.Gong, and Ch.Heng Lai Construction of a secure cryptosystem based on spatiotemporal chaos and its application in public channel cryptography // arXiv:nlin.CD/0502026 v1 11 Feb 2005
- [10] Gonzalo Alvarez Security problems with a chaos-based deniable authentication scheme // arXiv:nlin.CD/0412023 v1 9 Dec 2004
- [11] S.S. Chesnokov, A.A. Rybak Spatiotemporal Chaotic Behavior of Time-Delayed Nonlinear Optical Systems // *Laser Physics*, **10**, 3 (2000) 1
- [12] P. Pliszka, P.P. Banerjee Analysis of multifrequency dispersive optical bistability and switching in nonlinear ring cavities with large medium-response times // *Phys. Rev.* **A46** (1992) 507.
- [13] A.A. Balyakin, N.M. Ryskin Transition to Chaos in a Nonlinear Ring Cavity under Multi-frequency Driving // *Bull. Russian Acad. Sci.: Physics* **65** (2001) 1739.
- [14] A.A. Balyakin, N.M. Ryskin Chaotic Oscillations in Nonlinear Spatially-Extended Resonators // *Nonlinear Phenomena in Complex Systems* **4** (2001) 358.
- [15] V.E. Zakharov, E.A. Kuznetsov Hamiltonian Formalism for nonlinear Waves // *Usp. Fiz. Nauk* **167** (1997) 1137 [*Physics, Uspekhi* **40** (1997) 1087]
- [16] N.M. Ryskin, Coupled Nonlinear Schrödinger Equations for Describing the Propagation of Multi-frequency Wave Packets in a Nonlinear Medium with Dispersion // *Zh. Eksp. Teor. Fiz.* **106** (1994) 1542 [*JETP* **79** (1994) 833]
- [17] K. Ikeda, K. Kondo, and O. Akimoto Successive Higher-Harmonic Bifurcations in Systems with Delayed Feedback // *Phys. Rev. Lett.* **49**, (1982) 1467
- [18] Z. Hong, L. Yaowen, W. Yinghai, and H. Bambi Dynamics in a system with time-delayed feedback // *Phys. Rev.* **E 58**, (1998) 4383
- [19] Z. Hong, Z. Feizhou, Y. Jie, and W. Yinghai Nonlinear differential delay equations using the Poincaré section technique // *Phys. Rev.* **E 54**,(1996) 6925
- [20] E. M. Shahverdiev 1, R.A.Nuriev Parameter mismatches, variable delay times and synchronization in time-delayed systems // arXiv:nlin.CD/0404050 v1 28 Apr 2004
- [21] E. Ott, *Chaos in Dynamical Systems*, Cambridge University Press, 1993.

- [22] C. Grebogi, E. Ott, and J. A. Yorke, Chaotic Attractors in Crisis Phys. Rev. Lett. **48**, (1982) 1507
- [23] A.P. Kuznetsov, L.V. Turukina, E. Mosekilde Dynamical systems of different classes as models of the kicked nonlinear oscillator // Internat. Journ. Bifurcation and Chaos **11** (2001) 1065.
- [24] G.P. Agrawal, Nonlinear Fiber Optics, Academic, Rochester, New-York, 1989.